The enhancement of 21.2%-power conversion efficiency in polymer photovoltaic cells by using mixed Au nanoparticles with a wide absorption spectrum of 400 nm–1000 nm*

Hao Jing-Yu(郝敬昱)[a)†], Xu Ying(徐 颖)[a)†], Zhang Yu-Pei(张玉佩)[a)], Chen Shu-Fen(陈淑芬)[a)‡], Li Xing-Ao(李兴鳌)[a)], Wang Lian-Hui(汪联辉)[a)], and Huang Wei(黄 维)[a)b)]

[a)] *Key Laboratory for Organic Electronics and Information Displays and Institute of Advanced Materials (IAM), Jiangsu National Synergistic Innovation Center for Advanced Materials (SICAM), Nanjing University of Posts and Telecommunications, Nanjing* 210023, *China*

[b)] *Key Laboratory of Flexible Electronics (KLOFE) and Institute of Advanced Materials (IAM), Jiangsu National Synergistic Innovation Center for Advanced Materials (SICAM), Nanjing Tech University, Nanjing* 211816, *China*

(Received 20 September 2014; revised manuscript received 13 November 2014; published online 10 February 2015)

Au nanoparticles (NPs) mixed with a majority of bone-like, rod, and cube shapes and a minority of irregular spheres, which can generate a wide absorption spectrum of 400 nm–1000 nm and three localized surface plasmon resonance peaks, respectively, at 525, 575, and 775 nm, are introduced into the hole extraction layer poly(3,4-ethylenedioxythiophene):poly(4-styrenesulfonate) (PEDOT:PSS) to improve optical-to-electrical conversion performances in polymer photovoltaic cells. With the doping concentration of Au NPs optimized, the cell performance is significantly improved: the short-circuit current density and power conversion efficiency of the poly(3-hexylthiophene): [6,6]-phenyl-C60-butyric acid methyl ester cell are increased by 20.54% and 21.2%, reaching 11.15 mA·cm^{-2} and 4.23%. The variations of optical, electrical, and morphology with the incorporation of Au NPs in the cells are analyzed in detail, and our results demonstrate that the cell performance improvement can be attributed to a synergistic reaction, including: 1) both the localized surface plasmon resonance- and scattering-induced absorption enhancement of the active layer, 2) Au doping-induced hole transport/extraction ability enhancement, and 3) large interface roughness-induced efficient exciton dissociation and hole collection.

Keywords: Au nanoparticle, polymer solar cells, localized surface plasmon resonance, scattering, hole transport

PACS: 52.35.Hr, 52.25.Tx, 68.37.Lp, 68.37.Ps **DOI:** 10.1088/1674-1056/24/4/045201

1. Introduction

Organic photovoltaic (OPV) cells are attracting much attention due to their potential for low-cost and high-throughput processing. The absorption efficiency is one key problem to improve OPV's power conversion efficiency (PCE). In most polymers the "excitonic bottleneck" always brings a trade-off between light absorption and exciton harvesting efficiency since the light absorption depth is usually ∼10× larger than the exciton diffusion length (∼ 10 nm).[1] Bulk[2] and mixed[3] heterojunctions architectures or phosphorescent materials[4] are usually used to ease this exciton diffusion bottleneck. Even though this blended architecture has partially alleviated the problem of exciton dissociation in optically thick films, the internal quantum efficiency (IQE) in bulk heterojunction cells still diminishes rapidly with increasing the film thickness.[5] This drop in IQE particularly exerts a significant influence on many red and near-infrared (NIR) absorbing materials with low band gaps due to lower absorption coefficients than blue and green absorbers.[6] Another alternative method to improve absorption efficiency is to exploit the properties of surface plasmons (SPs).

SPs are electromagnetic surface waves confined to a metal–dielectric interface by coupling to the free electron plasma in metals, which are either localized around metal nanoparticles (noted with localized surface plasmon resonance, LSPR) or propagated as waves along planar metal surfaces. Ag and Au have played the leading role in this area although other metals also support surface plasmons. Up to now, many researchers have explored the influence of Au or Ag nanoparticles (NPs) or nanostructures on the solar cell performances by locating them into carrier extraction layer or active layer.[7–16] Au or Ag nanoparticles or nanostructures can be prepared with methods of laser ablation,[17] electron beam lithography,[18] focused ion beam milling,[9] nanosphere lithography,[19] scanning tunneling mi-

*Project supported by the National Basic Research Program of China (Grant Nos. 2015CB932202 and 2012CB933301), the National Natural Science Foundation of China (Grant Nos. 61274065, 51173081, 61136003, BZ2010043, 51372119, and 51172110), the Science Fund from the Ministry of Education of China (Grant No. IRT1148), the Specialized Research Fund for the Doctoral Program of Higher Education of China (Grant No. 20113223110005), the Priority Academic Program Development of Jiangsu Provincial Higher Education Institutions (Grant No. YX03001), and the National Synergistic Innovation Center for Advanced Materials and the Synergetic Innovation Center for Organic Electronics and Information Displays, China.

† These authors contributed equally to this work.

‡Corresponding author. E-mail: iamsfchen@njupt.edu.cn

© 2015 Chinese Physical Society and IOP Publishing Ltd

croscopy assisted nanostructure formation,[20] wet chemical synthesis,[21] etc. In all of the above approaches, wet chemical synthesis[21] is a good candidate due to the well dispersion of NPs in a variety of aqueous/organic solutions and the easy manipulation of NPs' size, shape, and density.[22]

The initial application of metal NPs in the OPV field is mainly focused on doping a single type of Ag or Au nanoparticles into OPV's carrier extraction layer or active layer.[7,8,13] In recent work, people have tried to use two types of NPs or the combination of metal NPs and nanostructures to enhance the cell's performance. For example, Li *et al.*[14] used dual plasmonic nanostructures including Au NPs and Ag nanogratings to broaden the absorption region and a ∼16% PCE enhancement factor was obtained with synergistic action of the 50-nm Au NPs and the 750-nm Ag nanogratings. At the same time, Hsiao *et al.*[23] introduced Au nanospheres (LSPR peaks of 520, 530, or 540 nm) and nanorods (longitudinal axis LSPR peaks of 660, 780, or 850 nm) into OPV cells to investigate the effects of the shape and size of Au nanospheres and nanorods on optoelectrical performances. The combination of Au nanospheres together with a type of Au nanorods generates two resonant peaks with its absorption extending from the visible to the near-infrared (NIR) region. By systematical analysis on film's extinction and photoluminescence (PL) spectra, they concluded that the integration of two kinds of Au NPs, covering the whole absorption band-edge of the active layer, is especially beneficial to the acquirement of the highest enhancement factor in OPV cells, which was also powerfully proved later by Lu *et al.* using a complementary absorption of Ag and Au nanospheres.[10] By utilizing the cooperative plasmonic effect of Ag and Au NPs, Lu *et al.*[10] realized a ∼19.6% PCE enhancement factor in their polymer solar cells that is far higher than 10.5% or 12.5% for the respective doping of Ag or Au NPs.

In this paper, we synthesize Au nanoparticles with the majority of bone-like, rod, and cube shapes and the minority of irregular spheres, and the mixture of these nanoparticles shows a broad absorption range of 400 nm–1000 nm. Their three main peaks of 525, 575, and 775 nm not only cover the main absorption region but also extend to the cutoff region of the poly(3-hexylthiophene) (P3HT):[6,6]-phenyl-C60-butyric acid methyl ester ($PC_{61}BM$) active layer. Scientific research demonstrates that the introduction of the mixed Au nanoparticles with an optimal doping concentration in the poly(3,4-ethylenedioxythiophene):poly(4-styrenesulfonate) (PEDOT:PSS) hole extraction layer brings a significant performance enhancement with factors of 20.54% and 21.2% for short-circuit current density (J_{sc}) and PCE, reaching 11.15 mA/cm^2 and 4.23%. The enhancement factors are rather high among the literature reports with metal NPs doped into the carrier extraction layer or directly spincoated onto the ITO electrode.[8,13,14]

2. Experiment

2.1. Synthesis of Au NPs

2.1.1. Preparation of seed solution

0.25 mL of a 10-mM aqueous solution of $HAuCl_4{\cdot}3H_2O$ was added to 7.5 mL of a 100-mM CTAB solution in a conical flask, and then stirred for 5 min. Next, 0.60 mL of an aqueous 10-mM ice-cold $NaBH_4$ solution was added. The solution turned pale brown–yellow with a vigorous mixture for 2 min and was maintained for 2 h in a water bath at 25 °C.

2.1.2. Preparation of growth solution

0.6 mL of a 10-mM aqueous solution of $HAuCl_4{\cdot}3H_2O$ was added to 14.25 ml of a 100-mM CTAB solution in a conical flask. Then, 210 μl of 10-mM $AgNO_3$ solution was added. The solution was gently mixed and stirred for 1 min. Then, 90 μl of 100-mM ascorbic acid (AA) was added and the mixture was homogenized by stirring gently for 10 s. Finally, the mixture solution became colorless.

Finally, 30 μl of seeded solution was added into the growth solution, and the whole solution was kept undisturbed for at least 3 h. Au NPs were centrifuged for about twice to remove reactants and stabilizing agents before use. The ultraviolet (UV) spectrum and the morphology for the Au NPs were measured with an ultraviolet-visible spectrophotometer (Shimadzu, UV-3600) and a transmission electron microscope (TEM) (Hitachi, HT7700), respectively. The PL spectra for the multilayer films were measured with a spectrofluorophotometer (Shimadzu, RF-5301PC).

2.2. OPVs fabrication and characteristics

Solar cells were fabricated on a 180-nm-thick indium tin oxide (ITO)-coated glass substrate. Pre-patterned ITO coated glass substrates (7 Ω·square^{-1}) were first cleaned with acetone, ethanol, and deionized water for 10 min in sequence and then blown with N_2. Before spin-coating Au NPs-doped PEDOT:PSS (AI 4083) layer or a control pure PEDOT:PSS layer, the substrates were treated with O_3 treatment for 3 min. The PEDOT:PSS or PEDOT:PSS:Au NP film was then dried at 100 °C for 10 min in a glove box with a thickness of ∼ 40 nm. Different Au NPs solutions were mixed with the PEDOT:PSS aqueous solution to generate different volume ratios of Au NPs to the PEDOT:PSS solution. The co-doping solution was continuously stirred for several hours before spin-coating the NPs-doped PEDOT:PSS film. The blend of P3HT (Rieke Metals 4002-E, 95–98% regioregular) and $PC_{61}BM$ (Solenne B. V.) with a weight ratio of 15 to 15 mg in 1 ml 1,2-dichlorobenzene (DCB) solvent was stirred at room temperature overnight. The blend layer was then spin-coated onto the PEDOT:PSS or NPs-doped PEDOT:PSS layer, forming a thick film of ∼ 70 nm.

The wet films were dried in covered glass petri dishes for about 1 h. The active layer-coated samples were then moved into the chamber in a glove box to thermally deposit a thin LiF and a thick Al as the cathode at 5×10^{-4} Pa. The current density-voltage (J–V) characteristics measurement was performed by using a source measure unit (Keithley 2400) under 100 mW·cm^{-2} illumination (AM 1.5 G, Oriel Sol3A, 300 W) in the atmosphere environment and room temperature without further encapsulation.

3. Results and discussion

The transmission electron microscope (TEM) image for these NPs is shown in Fig. 1. Having considered only the nanoparticle's shape, we find that our synthesis method is not good enough due to the occurrence of bone-like, rod, cube, and irregular sphere shapes. However, these mixed NPs generate a wide absorption spectrum covering the visible-to-NIR zone (Fig. 2(a)), which is very beneficial to the enhancement of PCE due to the concurrence of three LSPR peaks of 525, 575, and 775 nm. Here, we use finite difference time domain (FDTD) software from Lumerical Solutions Inc. to simulate the absorption cross sections around the bone-like, rod, and cube NPs, and the results are shown in Fig. 2(a). The simulation results demonstrate that the resonance peaks around 775 nm and 525 nm come mainly from the resonances of longitudinal and transverse axes of bone-like and rod-shape NPs. From the results in Fig. 2(a), one observes that one of the major absorption peaks in the absorption spectra is around 775 nm with a wide full width at half maximum (FWHM) (143 nm), far broader than 40 nm–50 nm of rods (the curves with left triangle and down triangle are for the rods with longitudinal and transverse axes of 40/14 nm and 46/12 nm, respectively) and 60 nm–70 nm of bone-like shapes (the curves with square, circle, pentagon, and up-triangle are for the bone-like shape NPs with longitudinal and transverse axes of 46/12, 45/12, 45/13, and 45/16 nm, respectively, and an edge width of 15 nm), so we conclude that the 775-nm peak is composed of some rod and bone-like shapes nanoparticles with a ratio range of 2.8–4.0. The 525-nm peak value corresponds to the resonance peak of the transverse axis for the rod and bone-like shape nanoparticles. In our simulation result, we cannot observe the resonance from the transverse axis mainly due to the assumption that all Au nanoparticles lie in the solution (with the longitudinal axis perpendicular to the incident light source) and this is not well matched with the real status of Au NPs (random distribution) in the water. In contrast, if we suppose that all of the Au NPs stand in the solution, that is, the longitudinal axis is parallel to the incident light source, then the intensity from the transverse axis is far higher than that from the longitudinal axis (not attached here). Another absorption peak of 575 nm comes mainly from cubes with side lengths of 27 nm–34 nm. Two absorption cross sections of cubes with side lengths of 28 nm and 32 nm are given in Fig. 2(a), from which we find that the resonance peakshift is not very obviously accompanied with the increase in the side length.

It should be pointed out that the above measured absorption spectrum is dispersed into aqueous solution, while for the case of the Au NPs in the cells, they are assembled onto ITO and covered with a poly(3,4-ethylenedioxythiophene):poly(4-styrenesulfonate) (PEDOT:PSS) hole extraction layer, so their absorption spectra will generate a redshift due to a refractive index of PEDOT:PSS ($\sim$ 1.5) larger than $\sim$ 1.3 of water. Thus, we simulate the absorption cross sections of some representative NP structures that occur in this paper, e.g., the bone-like Au NPs with longitudinal/transverse axes of 45/13 nm and an edge width of 15 nm, the rod ones with longitudinal/transverse axes of 46/12 nm and 40/14 nm, and the cube one with a side length of 32 nm. The absorption cross sections for these NPs in the PEDOT: PSS film are summarized in Fig. 2(b) and the simulation results indicate that Au NPs with longitudinal/transverse axis lengths of 45/13 (bone, square), 46/12 (rod, circle), 40/14 (rod, up triangle), and 32/32 (cube, down triangle) nm give redshifts of 53, 59, 57, and 65 nm, respectively, when changing ambient medium from aqueous solution to PEDOT:PSS. This means that the resonance peak of $\sim$ 575 nm in aqueous solution will move to $\sim$ 640 nm in the film, while the longitudinal resonant peak of $\sim$ 775 nm in aqueous solution will shift to $\sim$834 nm in the film, respectively corresponding to the absorption-edge region ($\sim$ 650 nm) and the cut-off zone ($>$ 700 nm) of the active layer P3HT: PCBM. According to the research results given by Hsiao *et al*,[23] Li *et al*.,[14] and Lu *et al*.,[10] the combination of two kinds of metal NPs or metal NPs with metal nanostructures with complementary absorption spectra is beneficial to the enhancement in OPV performance. Apart from this, as indicated by the analysis from Hsiao *et al*.,[23] the combination of NPs covering the whole absorption band-edge of the active layer is especially beneficial to the acquirement of a highest enhancement factor in OPV performance. Our mixed NPs cover not only the whole absorption band-edge of the active layer but also its cut-off region, indicating that both the absorption enhancement generated by the resonance and large scattering brought by large sizes of NPs will be beneficial to the performance enhancement in our solar cells.

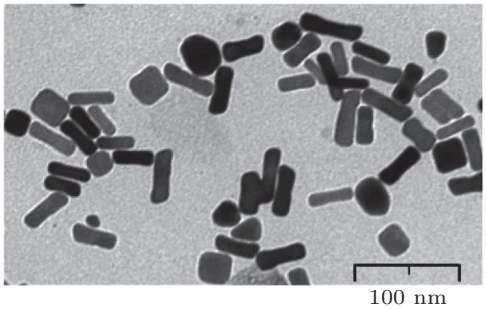


Fig. 1. The TEM image for the Au NPs used in this paper.

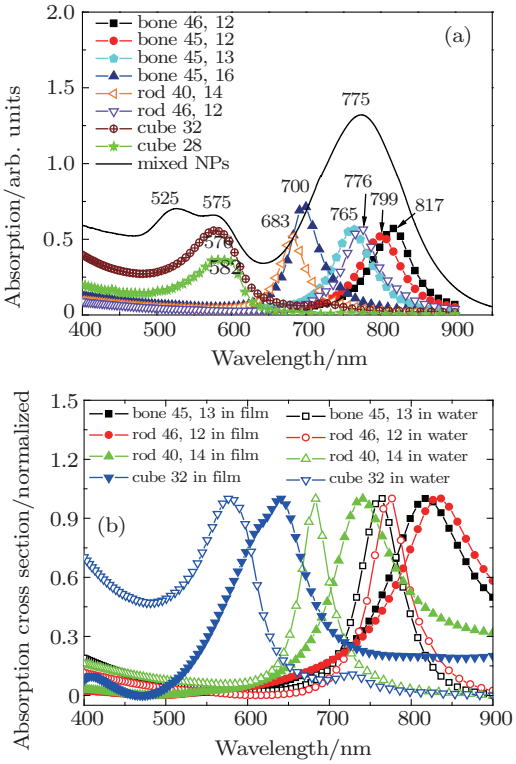


Fig. 2. (color online) (a) Measured and simulated absorption spectra of Au NPs. (b) Comparison of the absorption cross section between Au NP in the PEDOT: PSS film and that in water.

In order to observe the influence of the Au NPs on photovoltaic performances, a series of OPV cells is fabricated by doping the NPs into the PEDOT:PSS hole extraction layer. Here, the NPs with removing the residual reactants and the stabilizing agents, such as hexadecyltrimethylammonium bromide (CTAB) after being centrifuged several times, are finally controlled to be under a concentration of $\sim 10^{17}$ particles per ml in aqueous solution. The Au NP concentration in OPV device is further optimized to acquire the best OPV performance. The optimized ratio of NPs to PEDOT:PSS is around 4.5 vol%, the electrical performances for different NP concentrations of 3, 4.5, and 6 vol% under AM 1.5 G solar illumination condition are shown in Fig. 3(a). Here, the standard OPV device without doping any Au NPs is also given for comparison. From the J–V curves in Fig. 3(a) and the results that are summarized in Table 1, one finds that in the cell with an optimal doping concentration of 4.5 vol%, J_{sc} and PCE exhibit significant improvement factors of 20.54%, and 21.2%, increasing from 9.25 mA/cm^2 and 3.49% in the absence of Au NPs to 11.15 mA/cm^2 and 4.23%. When deviating from the optimization doping concentration, J_{sc} and PCE begin to decrease due to a higher reflectance of Au NPs to the incident solar light. With a low doping concentration (below 5%), the fill factor (FF) slightly increases, and then gradually declines with a further increase in the doping ratio, which is consistent with previously reported result.[24] The corresponding incident-photon-to-current conversion efficiency (IPCE) curves with different NPs doping concentrations (Fig. 3(b)) exhibit obvious improvement in a wide wavelength range of 400 nm–650 nm over that in the standard device, which is consistent with the above measured J–V characteristic and is similar to the previously reported results.[7,13,25]

Table 1. Device photovoltaic parameters with different Au NPs doping concentrations.

NPs concentration/vol%	V_{oc}/V	J_{sc}/mA·cm^{-2}	FF/%	PCE/%	R_s/Ω·cm^2
W/O	0.610	9.25	0.622	3.49	9.97
3	0.610	10.22	0.624	3.93	9.15
4.5	0.610	11.15	0.624	4.23	8.28
6	0.610	10.16	0.608	3.77	10.7

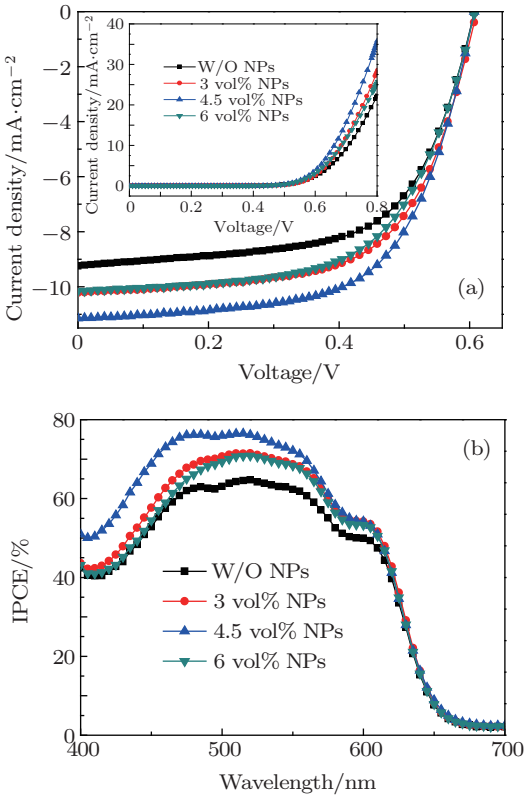


Fig. 3. (color online) J–V curves (a) and IPCE (b) of P3HT:PC$_{61}$BM devices with different Au NPs doping concentrations. Inset shows the dark current characteristics for all devices.

Photocurrent density (J_{ph})–effective voltage (V_{eff}) characteristic curves are calculated to observe photogenerated excitons. Here, J_{ph} is determined as $J_{ph} = J_L - J_D$, where J_L and J_D are, respectively, the current density under illumination and in the dark. V_{eff} is determined as $V_{eff} = V_0 - V_a$, where V_0 and V_a are the voltages at which $J_{ph} = 0$ and the applied bias voltage.[26] It clearly shows a linear increase of J_{ph} with V_{eff} at low V_{eff} values and then saturation at a high V_{eff} (i.e., $V_{eff} > 0.6$ V) in Fig. 4. Presuming that all the photogenerated excitons are dissociated into free charge carriers and gathered by electrodes at a high V_{eff} region, saturation current density (J_{sat}) is then only limited by the total number of absorbed incident photons. The G_{max} could

be calculated from $J_{ph} = qG_{max}L$, where q and L are the electronic charge and the thickness of active layer (70 nm). The values of G_{max} for the control device and devices with 3, 4.5, and 6 vol% NPs are 8.23×10^{27} $m^{-3}\cdot s^{-1}$ (J_{sat} = 92.17 A/m^2), 9.12×10^{27} $m^{-3}\cdot s^{-1}$ (J_{sat} = 102.1 A/m^2), 9.94×10^{27} $m^{-3}\cdot s^{-1}$ (J_{sat} = 111.34 A/m^2), and 9.06×10^{27} $m^{-3}\cdot s^{-1}$ (J_{sat} = 101.5 A/m^2), respectively. Because the value of G_{max} is determined only by the absorption of light,[7] the enhanced values suggest that the incorporation of the Au NPs increases the degree of light harvesting in the device, which is further testified with the significant enhancement in the absorption spectrum (Fig. 5(a)) for the multilayer film of PEDOT:PSS:NPs/P3HT:PC_{61}BM compared with the case of the control film of PEDOT:PSS/P3HT:PC_{61}BM around 400 nm–650 nm. From Fig. 5(a), we also observe that the absorption magnitude continues to increase with the increase in Au NPs concentration. This enhancement can be attributed to the absorption increase of the active layer and the PEDOT:PSS extraction layer induced by the LSPR of Au NPs. Figure 5(b) shows the absorption change in the PEDOT:PSS extraction layer. The test results show the absorption improvement of the PEDOT:PSS by incorporating Au NPs, indicating that part of the absorption improvement does not contribute to the photocarrier generation. However, compared with the absorption increase in the active layer, the increase is so weak that it can be neglected. So the main absorption enhancement comes from the active layer induced by the LSPR.

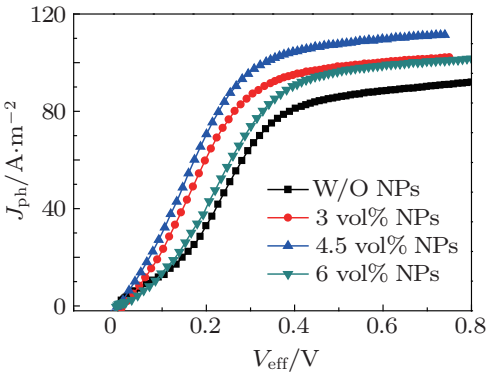


Fig. 4. (color online) Photocurrent densities versus effective voltage for the OPVs with different Au NPs doping concentrations.

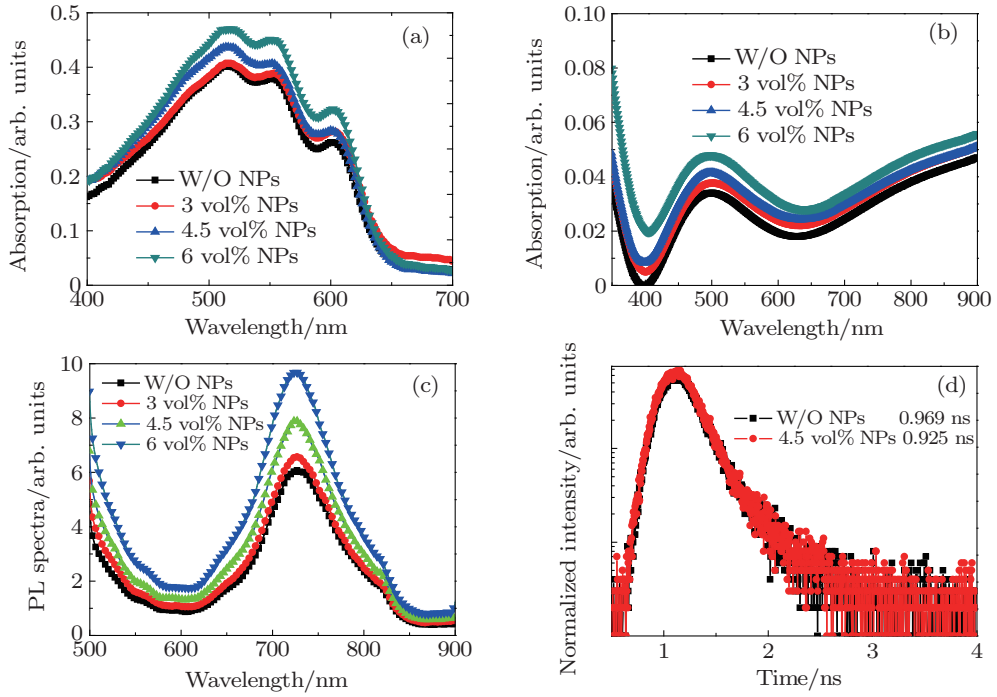


Fig. 5. (color online) Measured absorption (a) and PL spectra (b) of the PEDOT:PSS/P3HT:PCBM film with 3, 4.5, and 6 vol% Au NPs or without Au NPs incorporation. Measured absorption spectra of (c) PEDOT:PSS:NPs (3, 4.5, and 6 vol%) or without Au NPs incorporation. (d) The time-resolved photoluminescence spectra of PEDOT:PSS:NPs (4.5 vol%)/P3HT and the control film without NPs.

The measurements on the PL spectra also prove that the Au LSPR-induced absorption enhancement further induces a stronger PL intensity of the active layer, as shown in Fig. 5(c), which also indicates that Au NPs do not directly contact the active layer. In addition, it should be noted that although some Au NPs generate the LSPR beyond the absorption region of the active layer, e.g., $>$ 700 nm, the larger sizes also generate strong light scattering and result in lengthened light transport path, which further increases the light absorption in OPV cells. Figure 5(d) shows the measured time-resolved photoluminescence decay curves of the multilayer films of PEDOT:PSS:NPs (4.5 vol%)/P3HT and the control film without Au NPs. We calculate the exciton lifetime of P3HT after introducing Au NPs into the PEDOT:PSS hole extraction layer to be 0.925 ns, which is less than 0.969 ns for the intrinsic P3HT, indicating the effect of Au NPs on the excitons of the active layer.

Of course, other possible factors, e.g., the variations of the hole extraction and transport ability induced by Au NPs and the morphology changes of the PEDOT:PSS film with the incorporation of Au NPs may also influence the cell performances. In order to explore the influences of Au NPs on the hole extraction and transport ability of the PEDOT:PSS film, hole- and electron-dominated single-carrier devices with the structures of ITO/PEDOT:PSS ($\sim$ 40 nm, with 4.5% or without Au NPs)/Al and ITO/LiF (1 nm)/PEDOT:PSS ($\sim$ 40 nm, with 4.5% or without Au NPs)/LiF/Al are fabricated. The J–V curves shown in Fig. 6 indicate that the incorporation of Au NPs does not obviously affect the electron injection/transport ability of the PEDOT:PSS film, but their occurrence significantly improves the hole current in the hole-dominated device. This is attributed mainly to a slightly higher work function of Au (5.4 eV) than the highest occupied molecular orbital ($\sim$ 5.2 eV) of PEDOT:PSS, providing a fine hole injection at the ITO/PEDOT:PSS interface and simultaneously generating a shallow impurity energy level in the PEDOT:PSS film.[27]

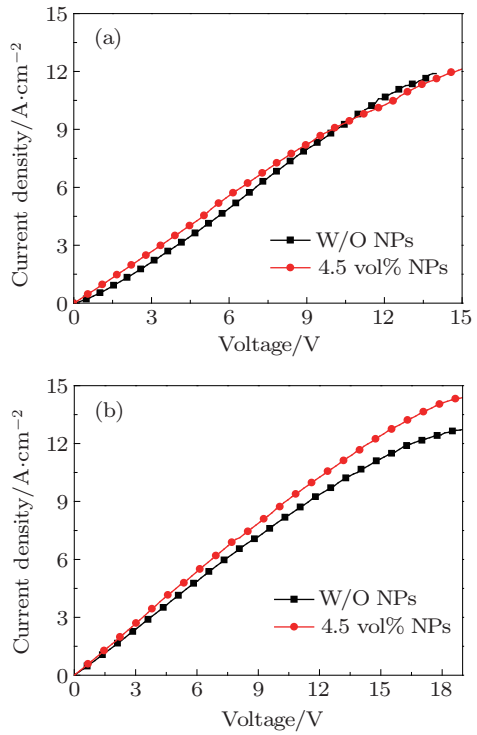


Fig. 6. (color online) The J–V characteristics for (a) single-electron and (b) single-hole devices.

Finally, as shown in Fig. 7, the morphology changes of the PEDOT:PSS layer with 4.5 vol% and without Au NPs are measured by atomic force microscopy (AFM) on the PEDOT:PSS or PEDOT:PSS:Au NPs film since it has been reported that increasing anode surface roughness will increase the interface area between the anode and the active layer, providing shorter routes for holes to travel towards the anode and enhancing hole collection at the anode.[28] The increased interfacial area between PEDOT:PSS and P3HT:PCBM allows the collection of a larger number of holes in the P3HT:PCBM layer, thus increasing J_{sc}. Besides, a rough P3HT:PCBM surface creates defect sites that assist exciton dissociation,[29] which is helpful to obtain a higher FF. By introducing the Au NPs, we observe a slight change of the surface morphology for the NPs-doped PEDOT:PSS film, with surface roughness (R_a) increasing from 1.05 nm to 1.11 nm. This result indicates that the doping of NPs is to some extent beneficial to exciton dissociation and the collection of a larger number of holes, resulting in the increase in J_{sc}, but we simultaneously infer that the roughness-induced increase in J_{sc} will not be significant due to a small variation of R_a.

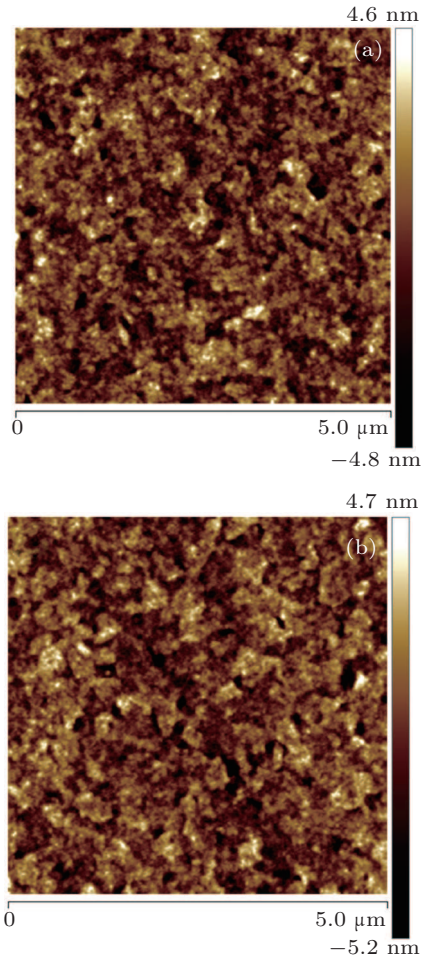


Fig. 7. (color online) Surface AFM images for (a) the pure PEDOT:PSS film ($R_a = 1.05$) and (b) 4.5-vol% Au NPs-doped PEDOT:PSS film ($R_a = 1.11$).

4. Conclusions

In this paper, Au NPs are synthesized and generate a wide absorption spectrum of 400 nm–1000 nm due to mixed bone-like, rod, cube, and irregular sphere shapes. These NPs are incorporated into the PEDOT:PSS hole extraction layer to improve optical-to-electrical conversion performances in polymer photovoltaic cells. The optimal doping concentration of Au NPs in PEDOT:PSS results in a significant performance enhancement with factors of 20.54% and 21.2% for

J_{sc} and PCE, reaching 11.15 mA·cm^{-2} and 4.23% for the P3HT:PC_{61}BM cell. Optical, electrical, and morphological changes brought by Au NPs are analyzed in detail and results demonstrate that the cell performance improvement can be attributed to a synergistic reaction, including: 1) the LSPR- and scattering-induced absorption enhancement of the active layer, 2) Au doping-induced hole transport/extraction ability enhancement, and 3) large interface roughness-induced efficient exciton dissociation and hole collection.

References

[1] Peumans P, Yakimov A and Forrest S R 2003 *J. Appl. Phys.* **93** 3693
[2] Halls J J M, Walsh C A, Greenham N C, Marseglia E A, Friend R H, Moratti S C and Holmes A B 1995 *Nature* **376** 498
[3] Xue J, Rand B P, Uchida S and Forrest S R 2005 *Adv. Mater.* **17** 66
[4] Shao Y and Yang Y 2005 *Adv. Mater.* **17** 2841
[5] You H L and Zhang C F 2008 *Chin. Phys. B* **18** 349
[6] Inganas O, Zhang F and Andersson M R 2009 *Acc. Chem. Res.* **42** 1731
[7] Chen F C, Wu J L, Lee C L, Hong Y, Kuo C H and Huang M H 2009 *Appl. Phys. Lett.* **95** 013305
[8] Wu J L, Chen F C, Hsiao Y S, Chien F C, Chen P, Kuo C H, Huang M H and Hsu C S 2011 *ACS Nano* **5** 959
[9] Chang Y C, Chou FY, Yeh P H, Chen H W, Chang S H, Lan Y C, Guo T F, Tsai T C and Lee C T 2007 *J. Vac. Sci. Technol. B* **25** 1899
[10] Lu L Y, Luo Z Q, Xu T and Yu L P 2013 *Nano Lett.* **13** 59
[11] Chen F X, Wang L S and Xu W Y 2013 *Chin. Phys. B* **22** 045202
[12] Yang J, You J B, Chen C C, Hsu W C, Tan H R, Zhang X W, Hong Z R and Yang Y 2011 *ACS Nano* **5** 6210
[13] Fung D D S, Qiao L, Choy W C H, Wang C, Sha W E I, Xie F and He S 2011 *J. Mater. Chem.* **21** 16349
[14] Li X, Choy W C H, Huo L, Xie F, Sha W E I, Ding B, Guo X, Li Y, Hou J, You J and Yang Y 2012 *Adv. Mater.* **24** 3046
[15] Li G L, He L J, Li J, Li X S, Liang S, Gao M M and Yuan H W 2013 *Acta Phys. Sin.* **62** 197202 (in Chinese)
[16] Li X, Choy W C H, Lu H, Sha W E I and Ho A H P 2013 *Adv. Funct. Mater.* **23** 2728
[17] Chen C D, Yeh Y T and Wang C R C 2001 *J. Phys. Chem. Solids* **62** 1587
[18] Felidj N, Aubard J, Levi G, Krenn J R, Salerno M, Schider G, Lamprecht B, Leitner A and Aussenegg F R 2002 *Phys. Rev. B* **65** 075419
[19] Li R, Zhu Y B, Di Y, Liu D X, Li B and Zhong W 2013 *Acta Phys. Sin.* **62** 198101 (in Chinese)
[20] Kolb D M, Ullmann R and Will T 1997 *Science* **275** 1097
[21] Jana N R, Gearheart L and Murphy C J 2001 *J. Phys. Chem. B* **105** 4065
[22] Murray W A and Barnes W L 2007 *Adv. Mater.* **19** 3771
[23] Hsiao Y S, Charan S, Wu F Y, Chien F C, Chu C W, Chen P and Chen F C 2012 *J. Phys. Chem. C* **116** 20731
[24] Chen X Q, Zuo L J, Fu W F, Yan Q X, Fan C C and Chen H Z 2013 *Sol. Energy Mater. Sol. Cells* **111** 1
[25] Kim S S, Na S I, Jo J, Kim D Y and Nah Y C 2008 *Appl. Phys. Lett.* **93** 073307
[26] Mihailetchi V D, Wildeman J and Blom P W M 2005 *Phys. Rev. Lett.* **94** 314
[27] Wang C C D, Choy W C H, Duan C, Fung D D S, Sha W E I, Xie F X, Huang F and Cao Y 2012 *J. Mater. Chem.* **22** 1206
[28] Hsu M H, Yu P, Huang J H, Chang C H, Wu C W, Cheng Y C and Chu C W 2011 *Appl. Phys. Lett.* **98** 073308
[29] Li G, Shrotriya V, Yao Y and Yang Y 2005 *J. Appl. Phys.* **98** 043704